

# Surveyor I: Preliminary Results

## Analysis and Evaluation of Data Returned during the Spacecraft's First Five Days on the Moon

Surveyor I soft-landed on the Moon at 061714 G.M.T., 2 June 1966. Presented is the preliminary analysis, made 5 days after touchdown, of scientific data already received.

Surveyor I landed on a dark, relatively smooth mare surface—a part of Oceanus Procellarum that is encircled by hills and low mountains. The crests of a few of these mountains, from which the spacecraft may be located accurately with respect to the major features of the lunar surface, are visible along the horizon. Observations of Sirius and of Canopus and of many points on the horizon show that the landing site is smooth and nearly level on a kilometer scale.

The terrain within 1 to 2 kilometers of the landing site is a gently rolling surface studded with craters, with diameters from a few centimeters to several hundred meters, and littered with fragmental debris ranging in size from less than 1 millimeter to more than 1 meter. The larger craters resemble those seen in the Ranger photographs in shape and distribution. Thus the landing site appears to be a representative sample of a mare surface.

The surface is composed of granular material of a very wide size range; coarse blocks of rock and smaller fragments are set in a matrix of fine particles too small to be resolved. This material was disturbed and penetrated by the footpads of the spacecraft to a depth of a few centimeters. The shapes of small craters suggest that the fragmental layer may extend to depths of at least 1 m.

The material disturbed by the footpads is made up of lumps that are probably aggregates of much finer grains—1 mm or less in diameter. These aggregates show that the local fragmental material is at least slightly cohesive. Some disturbed material was

thrown out to form rays, similar in shape and apparent genesis to those around some large craters observed from Earth; it is darker than the adjacent surface.

Thermal data, derived from comparison of predicted and actual temperatures, indicate that the spacecraft's temperature-control surfaces are not covered by dust.

If the material is homogeneous to a depth of some tens of centimeters, the soil has a static bearing capacity, on this scale, of about 5 pounds per square inch ( $3 \times 10^5$  dyne/cm<sup>2</sup>).

### Instrumentation

Surveyor is one of two current programs in unmanned lunar exploration supported by the National Aeronautics and Space Administration. It has three broad objectives: to demonstrate lunar soft-landing techniques, to obtain data on the lunar surface to assist the Apollo design, and to add to scientific knowledge of the Moon. The California Institute of Technology's Jet Propulsion Laboratory is responsible for project management; Hughes Aircraft Company,

This report was prepared by the Surveyor Scientific Evaluation and Analysis Team and associated working groups. To meet the scientific objectives of the Surveyor program, the Surveyor Scientific Evaluation and Analysis Team was established to provide a means to study the scientific data produced. In addition to the main Analysis Team, four associated working groups (Lunar Surface Mechanical Properties, Thermal Properties, Topography, and Electrical Properties) were formed to investigate in detail various aspects of the data. Analysis Team members include the investigators for later Surveyor missions, the Surveyor project scientist of the Jet Propulsion Laboratory, and the Surveyor program scientist of NASA. Members of the groups who contributed to the respective sections report are:

*Surveyor Scientific Evaluation and Analysis Team:* L. D. Jaffe, *chairman*, Jet Propulsion Laboratory; S. E. Dwornik, NASA Headquarters; W. M. Alexander, Temple University; S. A. Batterson, Langley Research Center; R. F. Scott, California Institute of Technology; E. M. Shoemaker, U. S. Geological Survey; G. H. Sutton, Columbia University; A. Turkevich, University of Chicago.

for Surveyor design and fabrication.

Surveyor I was the first of a series of engineering test models equipped with all subsystems necessary for soft landing on the Moon. It carried a survey television system and more than 100 items of engineering instrumentation, including temperature sensors, strain gages, accelerometers, and position-indicating devices; it carried no scientific experimental packages. The configuration of the spacecraft is shown in Fig. 1. Three hinged landing legs, with their associated landing pads and shock absorbers, were attached to a tubular aluminum structure. A vertical mast attached to the structure carried the commandable solar panel and high-gain planar-array antenna. Two thermally controlled compartments housed the communication equipment, power supply, and other electronic subsystems. Thermal control was accomplished by use of paint patterns, reflective surfaces, insulation, and variable thermally conductive paths between the interior of the compartments and their external radiating surfaces.

The solar panel supplied up to 85 watts of power; the two batteries aboard (one rechargeable) were used for energy storage and for handling peak loads. At launch, the spacecraft weighed approximately 2190 lb (mass, 1000 kg). After depletion of propellants and other consumables, and after jettison of an altitude-marking radar and the main retrorocket case, the landing weight decreased to about 600 lb earth weight (mass, 270 kg)—equivalent in the reduced lunar gravity to some 100 lb (450 newtons).

During cruise flight, inertial references were provided for the spacecraft by a Sun sensor, a Canopus tracker, and rate gyros; small nitrogen thrusters

*Lunar Surface Mechanical Properties:* S. A. Batterson, Langley Research Center; H. E. Benson, Manned Spacecraft Center; C. E. Chandler, Jet Propulsion Laboratory; E. M. Christensen, *chairman*, Jet Propulsion Laboratory; R. H. Jones, Hughes Aircraft Company; R. F. Scott, California Institute of Technology; E. N. Shipley, Bellcomm, Inc.; F. B. Sperling, Jet Propulsion Laboratory; G. H. Sutton, Columbia University.

*Lunar Surface Thermal Properties:* J. E. Conel, Jet Propulsion Laboratory; R. B. Erb, Manned Spacecraft Center; R. R. Garipay, Hughes Aircraft Company; W. A. Hagemeyer, Jet Propulsion Laboratory; J. W. Lucas, *chairman*, Jet Propulsion Laboratory; J. M. Saari, Boeing Science Laboratory.

*Lunar Surface Topography:* E. M. Shoemaker, U.S. Geological Survey; W. M. Alexander, Temple University; J. L. Dragg, Manned Spacecraft Center; E. C. Morris, U.S. Geological Survey; J. J. Rennison, *acting chairman*, Jet Propulsion Laboratory; A. Turkevich, University of Chicago.

*Lunar Surface Electrical Properties:* W. E. Brown, Jr., *chairman*, Jet Propulsion Laboratory; R. A. Dibos, Hughes Aircraft Company; D. O. Muhleman, Cornell University.

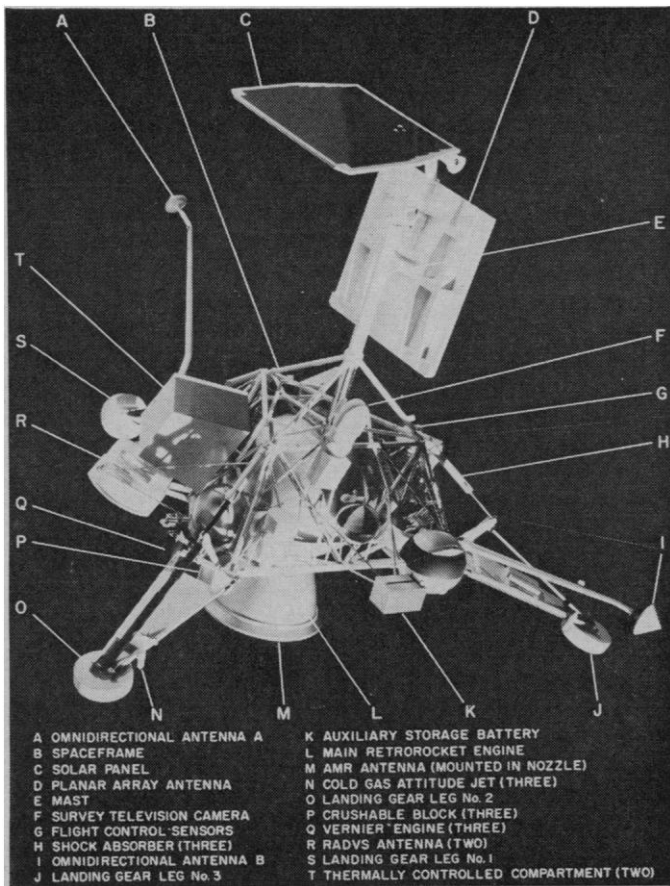


Fig. 1. Surveyor I spacecraft (A-21 model).

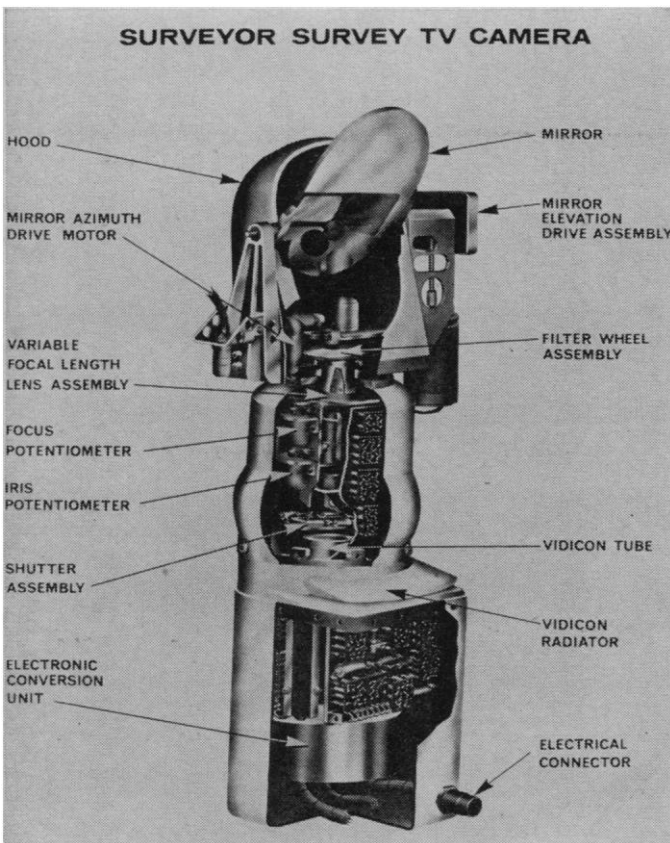


Fig. 2. Survey TV camera, Surveyor I.

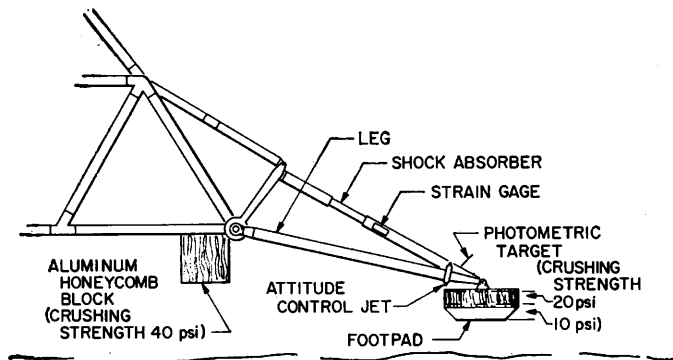


Fig. 3. Drawing of landing-leg assembly 2.

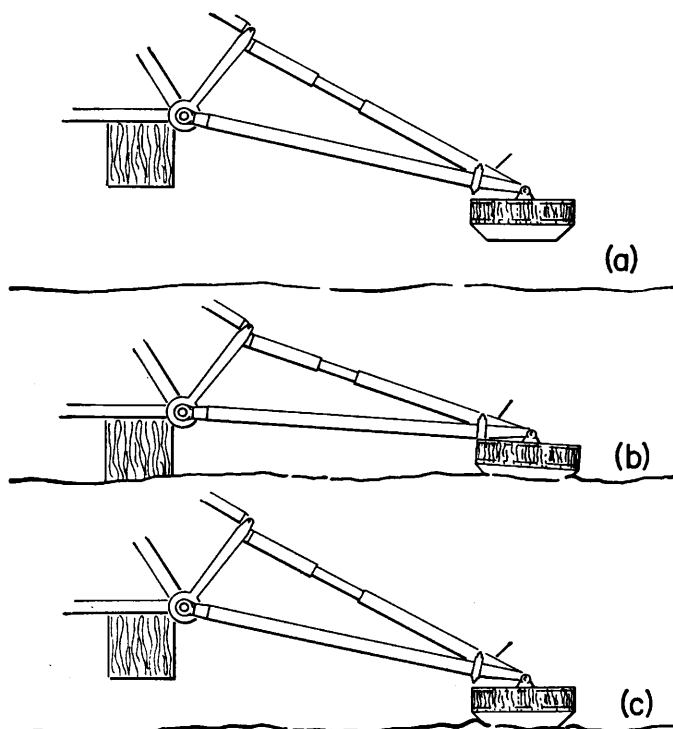


Fig. 4. Schematic of the Surveyor landing-leg assembly showing the articulation in a sequence of events during landing. In (a), the assembly is fully extended. During a landing, the shock absorber compresses and the footpad moves up and away from the spacecraft, as shown in (b). In (c), the assembly is shown re-extended after landing.

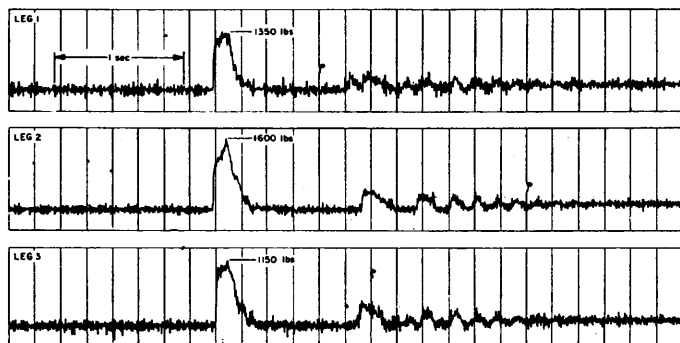


Fig. 5. Data from the shock absorber strain gages, as received at Goldstone, California. Note the oscillations following the primary impact.

exercised attitude control. During the terminal descent, the solid-fuel main retrorocket was ignited at a radar signal and burned for 40 seconds. Control during this and the final stages of the descent was exercised by a vernier propulsion subsystem that contained three continuously throttleable thrust chambers using hypergolic propellants; each chamber could deliver from 30 to 104 lb of thrust, and one could be gimballed for roll control. An on-board computer and autopilot supplied automatic closed-loop guidance for descent to touchdown, based upon radar measurements of altitude and velocity.

The telecommunications subsystem aboard the spacecraft included two transmitters, two receivers, two omnidirectional antennas, and one high-gain planar-array antenna. After the successful landing, the survey TV camera (Fig. 2) was activated to send 200- and 600-line pictures of the spacecraft and the lunar surface; the resolution attained is discussed later in this report. In the TV system, the vidicon tube, optics, shutter, filters, and iris were mounted along an essentially vertical axis, topped by a mirror that could be adjusted in both azimuth and elevation by command from Earth. The normal exposure, 150 msec, was extendible on command. Focal length of the optics was adjustable from 25 to 100 mm; the respective fields of view were 25.3 and 6.4 degrees square.

Launched from Cape Kennedy, Florida, 30 May 1966, Surveyor I was injected into a direct-ascent, lunar-intercept trajectory, performed a mid-course maneuver at 0645 G.M.T. 31 May, touched down at 061714 G.M.T., 2 June. The landing was made at 2.4° South, 43.4° West in the area north of Flamsteed crater in Oceanus Procellarum.

### Mechanical Properties

*Observations and explanations.* This interpretation of the lunar surface properties is based on photographs showing the area disturbed by the footpads and crushable blocks, and on the histories of the axial loads in the shock absorber on each of the three legs during the landing (Fig. 1). Important components of the landing-gear assembly appear in Fig. 3, and their motions during landing are illustrated schematically in Fig. 4. The spacecraft landed at a vertical velocity of about 10 ft/sec (3 m/sec), with a small component of horizontal velocity; there is now un-

certainly of several feet per second in all the velocity information.

Figure 5 shows the time records of the axial load as measured by a strain gage on each shock absorber; the fact that surface contact by all three footpads was almost simultaneous indicates that the spacecraft mast (Fig. 1) was approximately normal to the surface at touchdown. The footpads impacted at intervals of 0.01 second; No. 2 touched first, followed by No. 1 and then by No. 3.

After primary impact the spacecraft rebounded clear of the surface; occurrence of a secondary impact approximately 1.0 second after the initial impact indicated that the footpads rebounded about 2½ inches (6 cm) above the surface. The second impact developed maximum loads of approximately 25 percent of the maximum loads developed during the initial impact. The maximum vertical load applied to the footpads by the lunar surface during initial impact was 400 to 500 lb (1800 to 2300 newtons). Conversion of this load to a dynamic pressure applied to the surface depends on the footpad area in contact with the soil at the instant the load was measured; since the lower portion of the footpad is a truncated cone (Fig. 3), this contact area depends primarily on the depth of penetration. Based on the maximum vertical load and the footpad areas, a unit loading of between 4 and 10 lb/inch<sup>2</sup> (3 to 7 × 10<sup>5</sup> dyne/cm<sup>2</sup>) was applied to the surface during the dynamic stages of the impact. The static load required to support the spacecraft on the three landing pads is about ½ lb/inch<sup>2</sup> (4 × 10<sup>4</sup> dyne/cm<sup>2</sup>).

Based on preliminary velocity and spacecraft performance data, analytical simulations of the landing dynamics have been performed. To date, for simulated landings on a rigid surface, force levels have been duplicated within 10 percent. However, the timing of all events during the landing, as indicated by the strain-gage data (rise time of force, rebound, reimpact, and durations of force during first and second impact), can be duplicated as precisely as the data allow it to be read out. The design of the spacecraft landing gear is such that the forces and motions of the craft are largely independent of the mechanical properties of the surface for surface materials whose static bearing capacity is greater than approximately 5 lb/inch<sup>2</sup> (4 × 10<sup>5</sup> dyne/cm<sup>2</sup>). Fur-

ther discrimination of the material properties can be obtained from analyses of the footpad penetration.

A number of oscillations with a maximum peak-to-peak amplitude of several hundred pounds and a frequency near 7 cy/sec are seen to follow the second impact (Fig. 5). The oscillations of the forces in all the shock absorbers are in phase and of about equal amplitude, indicating a rectilinear vertical mode. The frequency of the oscillations is related to the elasticity of the spacecraft structure and the lunar surface material.

A picture of a depression in the lunar surface under (cylindrical) crushable block 3 (Fig. 6) indicates that it also made contact with the lunar surface. At the time of writing, it has not been possible to identify positively any lunar surface depression under crushable block 1. The area beneath crushable block 2, and the crushable blocks themselves, cannot be seen by Surveyor's TV camera, but the symmetry of the impact and the general local flatness of the lunar surface lead to the assumption that all the crushable blocks made contact with the lunar surface. Measurements of shadows of the depression made by crushable block 3 indicate a depression depth of about ¾ inch (2 cm).

Pictures of each footpad confirm the nature of the landing expressed by the dynamics data. Pad 2 (Fig. 7) and pad 3 (Fig. 8) are both visible; pad 1 is not. The appearance of the lunar surface near pads 2 and 3 indicates similar behavior of the material displaced by the two pads; they appear to have landed in granular material, to have extended laterally during impact (Fig. 4), forcing the surface material away, and then to have drawn back on the rebound to their final position, leaving a disturbed region of the surface.

There is no evidence to indicate crushing of the conical section of the footpad. At least the visible part of the lower layer, made of aluminum honeycomb material having a crushing strength of 10 lb/inch<sup>2</sup> (7 × 10<sup>5</sup> dyne/cm<sup>2</sup>), is undamaged (Fig. 9). No crushing of the upper layer of crushable structure (crushing strength, 20 lb/inch<sup>2</sup> or 1 × 10<sup>6</sup> dyne/cm<sup>2</sup>) took place. It should be noted that, at the landing velocity of approximately 10 ft/sec (3 m/sec), preflight analyses showed that no crushing of the footpads would occur even on a rigid surface; this finding indicates that dynamic

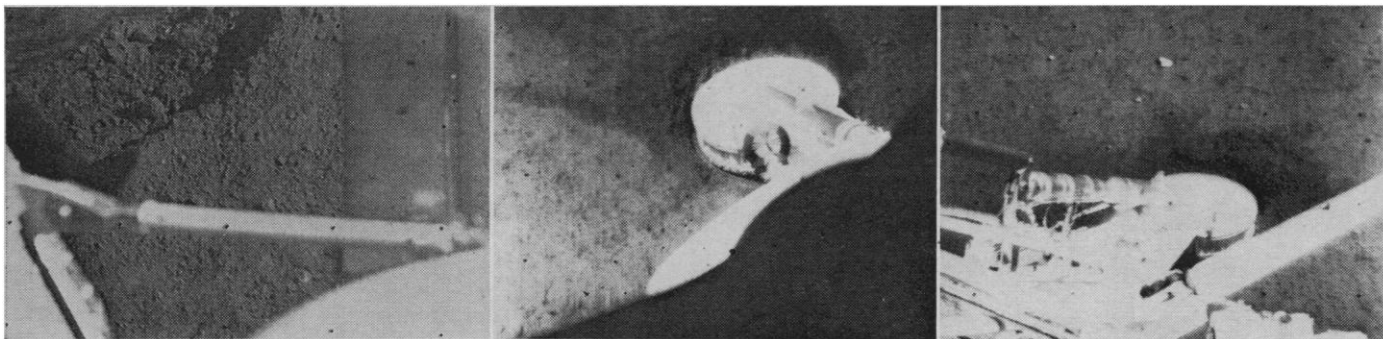


Fig. 6 (left). Surface depression (upper left-hand corner) made by crushable block 3. Some parts of the spacecraft are shown. This photograph has been digitized and corrected by computer for frequency response of the television systems. Fig. 7 (center). Wide-angle photograph of footpad 2. Note the displaced material that covers the lunar surface beyond the footpad, and the ray extending to the left from the footpad. Fig. 8 (right). Wide-angle photograph of footpad 3. Note the similarity of the throwout material to that shown in Fig. 7.

pressures of 10 lb/inch<sup>2</sup> on the footpads during landing were not exceeded and that the footpad did not crush, but displacement of the granular lunar surface material did occur. The shock-absorber data, discussed above, are in agreement with this evaluation.

At both pads 2 and 3 there is a throwout over the surface (see Figs. 7 and 8), including rays of apparently fine-grained material, to a distance of a foot or two from the edge of the pad. Nearer the pad, the surface material is pushed up by the impact to form a raised rim. The side of the depression and the rim have a chunky or blocky appearance (Fig. 10); the blocks or clumps of material are irregular, range in size, and appear to consist of aggregates of fine-grained material rather than of individual stones or pebbles. The basic grain size is quite small and below the limit of resolution of the narrow-angle pictures in the

600-line mode; the limit is about 0.02 inch (0.5 mm) at the distance of pad 2.

Movements of pad 2 during landing caused some small deformations of the surface adjacent to the pad on the side nearest the camera (Fig. 11). The deformations resulted in an irregular pattern of cracks or fissures at the surface of the material. The pictures of pad 2 (for example, Fig. 7) clearly show that its cylindrical part lies above the level of the undisturbed surface. The penetration of pad 2, in the final location, was calculated from shadow measurements on two photographs taken 69 hours apart; the measurements indicate that the base of the footpad, if it is uncrushed, lies about 1 inch (25 mm) below the adjacent undisturbed surface.

Until a detailed study of the depression caused by the pad is completed, one cannot say to what extent the lunar surface material was in fact compressed in volume by the impact. It

is certain that the craters caused by the pad impacts did not result entirely from volumetric compression, and that some displacements of the material did occur.

To determine whether any surface erosion could be caused, the attitude-control jet on leg 2 (Fig. 3) was operated after landing. This jet uses cold gaseous nitrogen to produce a thrust of 0.06 lb; it is located approximately 6 inches (15 cm) from, and at an angle of 72 deg to, the surface. Pictures were taken before, during, and after the firings, which consisted of short pulses repeated for periods of up to 4.5 seconds. Duration of the pulses was 20 msec, with a 30-msec pause between pulses. Results of this experiment are as yet inconclusive, since the initial study of the pictures taken before and after the firings did not indicate any obvious soil disturbance; more detailed study remains to be made.

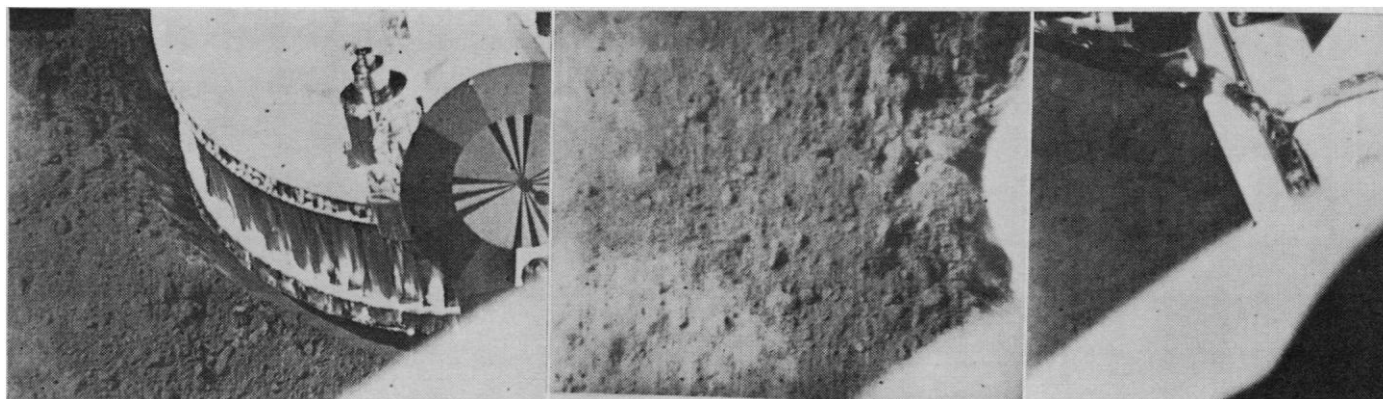


Fig. 9 (left). Narrow-angle photograph of footpad 2. The upper part of the pad is made of honeycomb structure with a crushing strength of 20 lb/inch<sup>2</sup> ( $1 \times 10^6$  dyne/cm<sup>2</sup>). The lower part has a crushing strength of 10 lb/inch<sup>2</sup> ( $7 \times 10^5$  dyne/cm<sup>2</sup>). This photograph has been digitized and corrected by computer for frequency response of the television systems. Grains of 0.5 m can be resolved in the disturbed surface next to the footpad. Fig. 10 (center). Narrow-angle photograph of the disturbed lunar material beyond footpad 2, the circular object at the bottom of the picture. Fig. 11 (right). Narrow-angle photograph of the disturbed lunar surface material near footpad 2. The pad is in the upper portion of the photograph with a landing leg extending downward. The surface shown lies between the footpad and the spacecraft.

*Interpretations.* The appearance of disturbed surface material and the rim of the impact depression suggest that the surface is a granular soil-like medium of unknown but fine grain size and size range. On disruption by the impact, some fine-grained material was thrown out in a spray, possibly from an original surface layer, and the underlying material was fragmented to some extent. The behavior of the material is consistent with its having a distinct but small amount of cohesion; its manner of deformation appears to be qualitatively similar to that which might be exhibited by a terrestrial damp, fine-grained soil.

The appearance of the lunar surface and the nature and depths of the depressions formed during landing are very similar at pads 2 and 3, so that, at least to the scale of Surveyor, the material properties appear to be horizontally homogeneous. If, to a depth of the order of the footpad diameter (1 ft or 30 cm), the material is homogeneous and similar to that observed at the surface, a simplified landing-dynamics analysis indicates that the soil has a static bearing capacity, at the scale of the Surveyor footpad, of about 5 lb/inch<sup>2</sup> ( $4 \times 10^5$  dyne/cm<sup>2</sup>) and a friction angle between 30 and 40 deg at a density of terrestrial soil (3 slugs/ft<sup>3</sup> or 1.5 g/cm<sup>3</sup>).

However, the landing-dynamics data, penetration observations, and landing simulations performed to date are also compatible with a lunar surface consisting of a hard material (static bearing capacity greater than 10 lb/inch<sup>2</sup> or  $7 \times 10^5$  dyne/cm<sup>2</sup>) overlain by a weaker material to a depth of about 1 inch (25 mm).

#### Thermal Properties

*Earth-based observations.* The landing site of Surveyor I, 2.4°S, 43.4°W, is contained in the Lunar Isothermal Chart (1). The site is in a "bland" area in that local surface-temperature gradients across the surface during lunar eclipse are small; this is typical of the major portion of the visible lunar surface. Another characteristic of these typical areas is that the surface exhibits a high value (of the order of 800 cgs units) of the thermal parameter  $(k\rho c)^{-1}$ ,

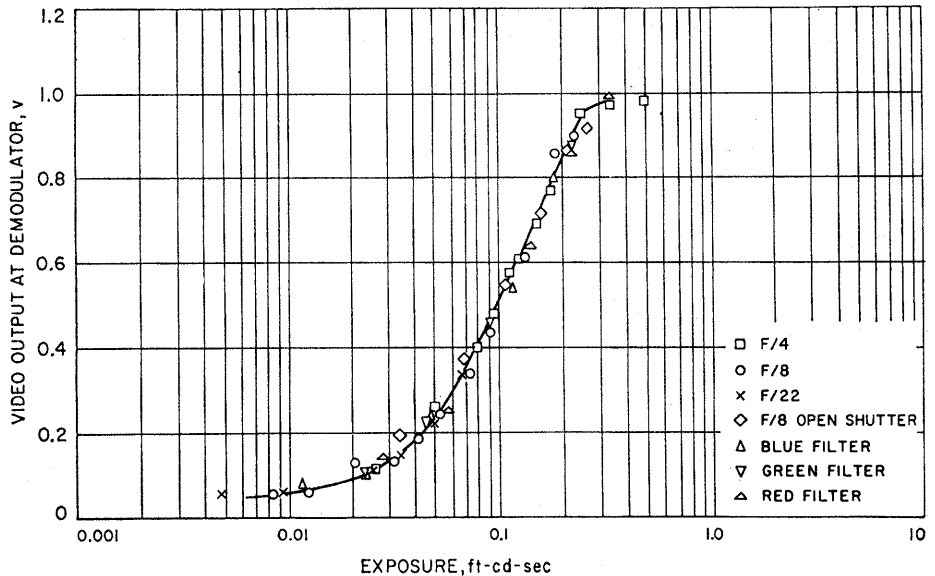


Fig. 12. Calibration data for the Surveyor I television camera illustrating dynamic range.

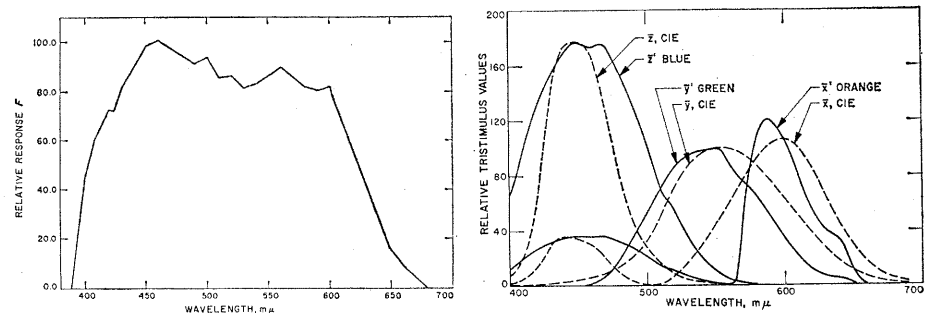


Fig. 13 (left). Spectral response curve of the Surveyor I television camera, at the clear position of the filter wheel. Fig. 14 (right). Graph of the overall camera-filter spectral response illustrating the fit to the standard C.I.E. (Commission Internationale de l'Éclairage, 1931) color-matching functions. The second maximum in the  $\bar{x}'$  curve is obtained from a reduced value of the  $\bar{z}'$  function added to the original  $\bar{x}'$  camera-filter response. Solid lines are camera-filter response curves; dashed lines are C.I.E. color-matching function.

where  $k$  is thermal conductivity,  $\rho$  is density, and  $c$  is specific heat. For purposes of comparison, an evacuated powder consisting of 1- to 25- $\mu$ -sized particles of olivine, tektite, or granodiorite has a thermal parameter in this range (2). It is interesting to note that the measured bearing strength of such powders is sufficient to be consistent with the resting of Surveyor I on the lunar surface (3). Further, the site is in a relatively dark area, where the albedo or solar reflectance is lower than average; J. M. Saari estimates the local albedo to be 0.052.

*Observations based on spacecraft data.* A rather firm conclusion can be drawn from temperatures at many locations throughout the spacecraft during its operation on the lunar surface; the temperatures are at levels to be expected with clean external thermo-

radiative surfaces. This fact strongly indicates that the surfaces bear essentially no dust. It should be noted that thermal conditions of the lunar surface have little effect on temperatures at most locations in the spacecraft because the underside of the craft has a highly reflective metallic surface.

The temperatures of a few of the external surfaces on Surveyor I are determined primarily by heat exchange with the lunar surface and with deep space. These surfaces are rather well insulated, as to both conduction and radiation, from the remainder of the spacecraft. The portion of the lunar surface that determines the spacecraft temperatures is very localized: 80 percent of the radiation view factor from the selected spacecraft surface to the Moon consists of approximately 1000 ft<sup>2</sup> (100 m<sup>2</sup>) adjacent to the spacecraft.

A very preliminary estimate of the lunar-surface brightness temperature at 1200 G.M.T., 2 June 1966, is 180°F (4); this estimate, based on measured temperatures in the spacecraft, is for the appropriate Sun-elevation angle of

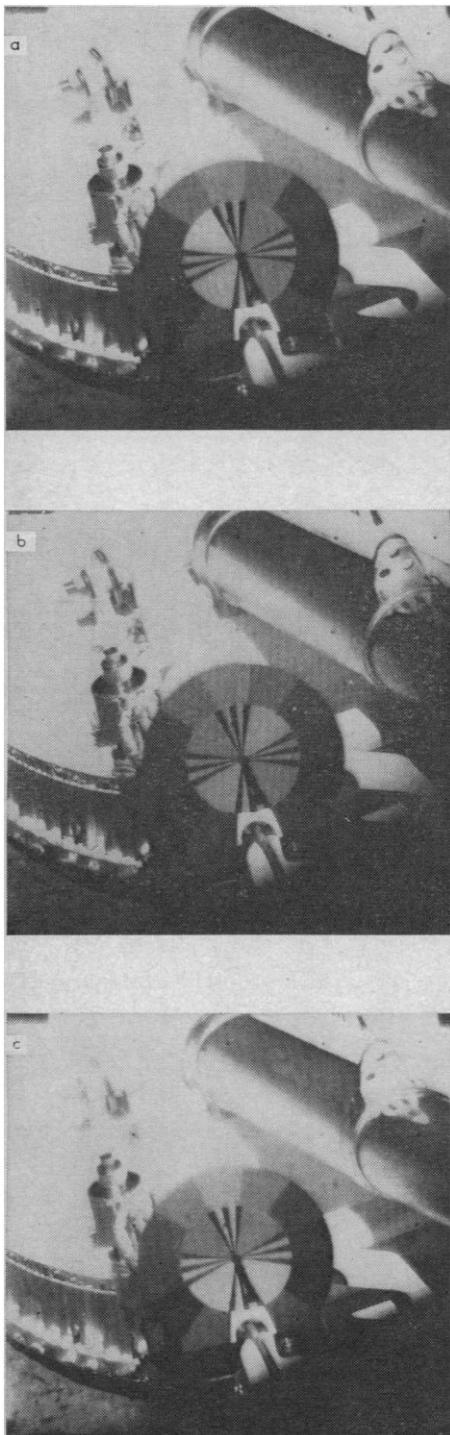


Fig. 15. Photometric target on footpad 2 of the Surveyor spacecraft. The target is used for photometric calibration of the television camera during lunar operation. Frame (a) is observed through  $\bar{x}$  filter; (b) is observed through  $\bar{y}$  filter; and (c) is observed through  $\bar{z}$  filter.

31 deg and an assumed lunar-surface thermal emittance of 1.0. The value of 165°F may be compared with a preliminary prediction of a local lunar-surface brightness temperature of 120°F derived from Earth-based measurements and assuming a thermally smooth lunar surface. Simplified thermal models of both the spacecraft and the lunar surface were used in making these estimates. Much more detailed analysis is necessary before it can be confirmed that the local surface temperature of the Moon, at the landing site but without effects introduced by the spacecraft, is higher than the average for that portion of the Moon. At present it appears that using a thermally rough lunar surface and taking its directional characteristics into account will result in an expected lunar surface temperature, as seen by the selected spacecraft temperature, rather close to 180°F.

#### Surface Topography

Four thousand pictures were taken by the television camera aboard Surveyor I during the first 5 days after landing. During this period the lunar surface was observed through Sun-elevation angles ranging from 28 to about 88 deg. An immense quantity of detailed information about the local lunar surface is contained in the pictures; we report here the first scientific results yielded by the lunar forenoon and noon photographs.

The television camera was operated in two modes: one in which the picture is composed of 200 television scan lines, and a second higher-resolution mode in which the picture is composed of 600 scan lines. A total of 14 pictures in the 200-line mode and 3986 in the 600-line mode were obtained. The 600-line television pictures are of superior quality and may be compared favorably with the lunar television pictures acquired by the Ranger spacecraft. The Surveyor pictures are exceptionally free of coherent noise and show very little shading of the field because of the relatively uniform response of the vidicon target.

The calibrated angular resolution of the Surveyor camera ( $\frac{1}{2}$  mr at 15-percent relative response) is approximately half the angular resolution of the average human eye. The ground resolution near one of the spacecraft footpads, 1.6 m from the camera, as measured from pictures for which the modulation transfer function has been

compensated (Fig. 9), is about 0.5 mm; higher ground resolution can be achieved directly beneath the camera. It is of interest to note that the highest resolution obtained in the Ranger pictures represents an improvement over the best resolution of the lunar surface achieved by telescope by three orders of magnitude, and that the Surveyor pictures represent a gain in resolution over the highest-resolution Ranger pictures by three more orders of magnitude. The Surveyor I pictures show significantly better resolution than the pictures acquired earlier this year by the Soviet spacecraft Luna 9.

The total range of response of the Surveyor I camera is about 1 million to 1, enabling its use for recording stars as faint as sixth magnitude, on the one hand, and for photographing the brightest parts of the lunar surface on the other. Thus, the dynamic range of the camera is within a factor of ten of the dynamic range of the human eye.

The photometric response of the Surveyor I camera on the Moon, observed by means of repeated pictures of a photometric calibration target mounted on a leg of the spacecraft, has proved to be fairly stable and close to the response observed in preflight calibration. In its normal mode of shutter operation, which provides a 150-msec exposure, the total dynamic range of the vidicon tube is approximately 25 to 1; the logarithm of the video voltage is nearly a linear function of the log lunar scene luminance over a range of about 5 to 1 (Fig. 12).

Table 1. Categories of television pictures taken during lunar forenoon and noon.

Pictures	Approximate number of frames
200 lines	14
600 lines	
Wide-angle frame panoramas	390
Narrow-angle frame panoramas	1160
Wide-angle frame panoramas with color filters	870
Narrow-angle frame panoramas with color filters	1160
Footpad survey	100
Crush block imprint survey	30
Gas jet experiment	30
Star survey	20
Photometric and color calibration target	100
Study of objects of special interest and verification frames for aperture, focus, and position	126

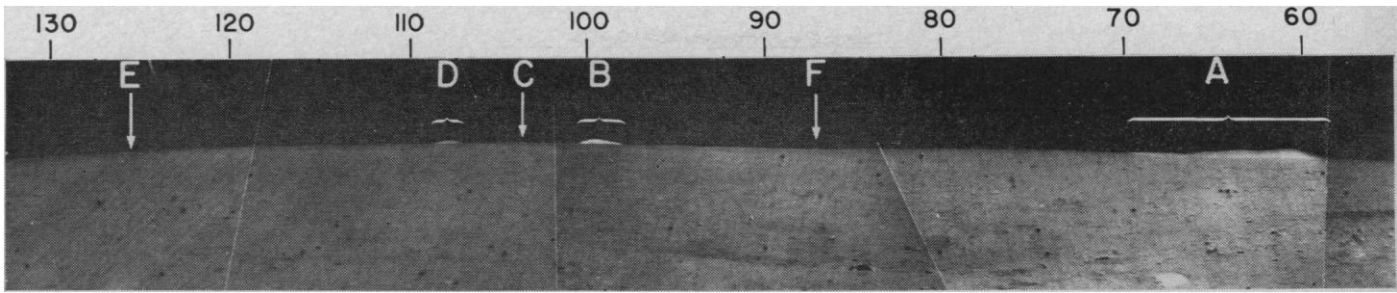


Fig. 16. Wide-angle panorama of the lunar horizon in the northern quadrant as observed by Surveyor I. The region covered is from 55 to 130 degrees azimuth (camera coordinates); sun elevation is approximately 50 degrees. Most of the curvature of the horizon arises from the nonvertical mounting of the camera.

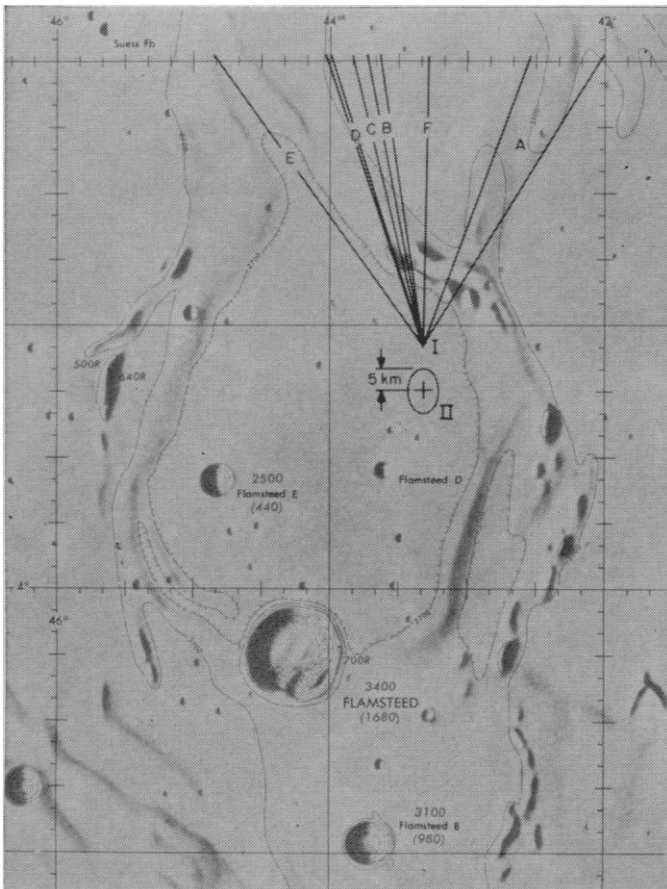


Fig. 17 (above). Surveyor I landing sites as deduced from horizon features. Two sites that seem compatible with these features are shown. Site II coincides with the site deduced from trajectory tracking data. The ellipse around site II is the  $2\sigma$  error. [Base map, ACIC Lunar Chart LAC 75]

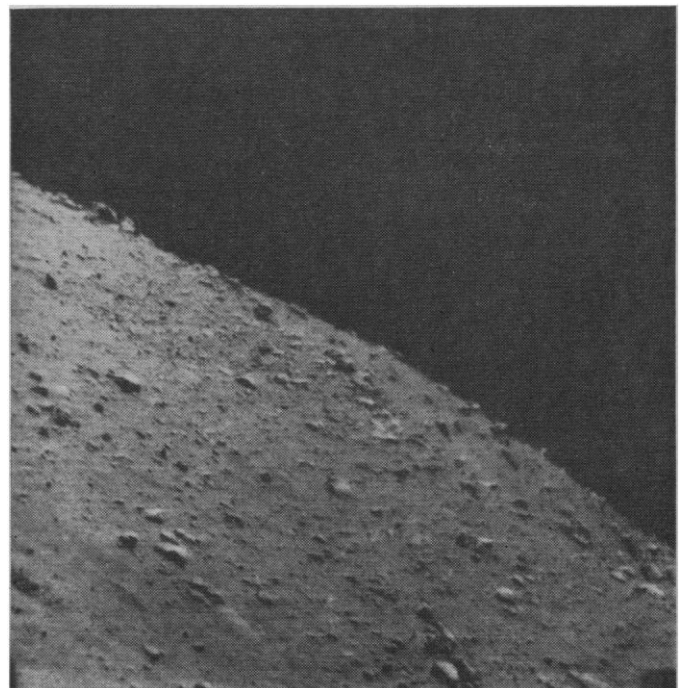


Fig. 18 (upper right). Sector of rim of large crater on horizon, southeast of the spacecraft. Coarser blocks are probably more than a meter in width.

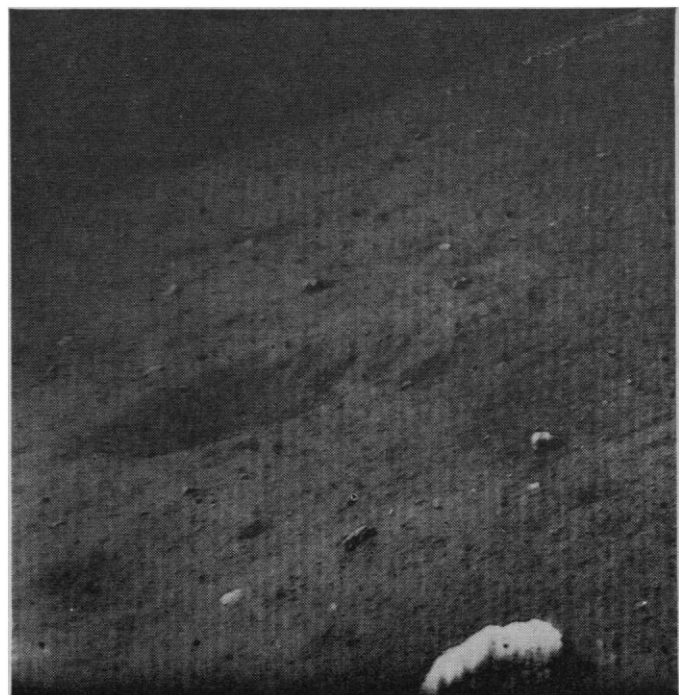


Fig. 19 (lower right). Crater approximately 3 m in diameter, southeast of spacecraft.

Table 2. Characteristics of horizon features.

Feature	Location (deg)		Width visible		Maximum height visible	
	Camera coordinate	Approximate selenographic coordinate	deg	km*	deg	m*
A	65	N27°E	11.2	2.54	0.44	100
B	98	N 6°W	2.5	0.79	0.24	75
C	102	N10°W	0.3		0.08	
D	107	N13°W	1.5	0.52	0.15	52
E	124	N32°W	0.5		0.12	
F	88	N 3°E	0.5	0.15	0.04	10

\* Figures are for the parts visible over the horizon. They are calculated on the basis of the site I location (see text).

The great dynamic range of the camera system is achieved by means of an iris, by filters in the optical train, and by alternate modes of shutter operation and electron-beam scanning cycle: by use of the variable iris aperture, which provides nominal focal ratios ranging from  $f/4$  to  $f/22$ , the dynamic range of the camera is increased from 25 to 1 to somewhat more than 800 to 1; rotation into the optical train of color filters on a camera filter wheel can be used to increase further the dynamic range to about 3,000 to 1; by use of a 1.2-second exposure (open-shutter mode) the dynamic range of

the camera can be extended to about 25,000 to 1; finally, the sensitivity of the camera to very faint objects can be increased still further, by a factor of about 40 over the open-shutter mode, by means of several minutes' exposure (integration mode).

The color filters in the camera filter wheel were selected so that the overall camera-filter spectral response (Fig. 13) would match the standard color-matching functions of colorimetry as well as is possible with single filters (Fig. 14). In order to maintain colorimetric calibration and enhance the detection of color differences, the photometric target

is equipped with three colors of purity and dominant wavelength that bound the gamut of normal rock colors. Figure 15 shows the appearance of the target as seen on the lunar surface through the three color filters.

The lens assembly of the Surveyor television camera provides a variable focal length ranging from 25 to 100 mm. The camera is normally operated at either the long or short focal-length extremum: the 25-mm focal length resulting in a 25.3-deg optical field of view; the 100-mm focal length, in a 6.4-deg field of view. For convenience we refer to the former as a wide-angle frame and to the latter as a narrow-angle frame.

The camera has been operated to provide a wide variety of information (Table 1). Several wide-angle frame panoramas have been taken of the lunar scene on different days and with different color filters. (A complete wide-angle frame panorama requires about 120 frames.) Several sectors of the complete panorama have also been taken in narrow-angle frames on different days and with color filters (a complete narrow-angle frame panorama requires nearly 1000 frames). Surveys of two of the spacecraft footpads, and of imprints on the lunar surface left by the crushable blocks beneath the frame of the spacecraft, have been conducted on each successive day. On 2 days, the attitude-control jets mounted on the legs of the spacecraft were fired to see whether the gas emitted would disturb the surface; the effects were sought from comparison of television pictures taken during and after the firing of the jets with pictures taken before. Repeated photographs were taken of the photometric and color-calibration target each day to provide control for the photometric reduction of the pictures. Finally, several objects of special interest, such as large rocks close to the spacecraft, were examined with additional photographic coverage in order to obtain maximum information on the shape, texture, and color of these objects.

In order to measure the photometric function of the local lunar surface and various objects on the surface, and to map the surface topographically by use of shadows and by photometric techniques, it is necessary to survey the surface repeatedly at different positions of the Sun; different kinds of information are provided about the surface,

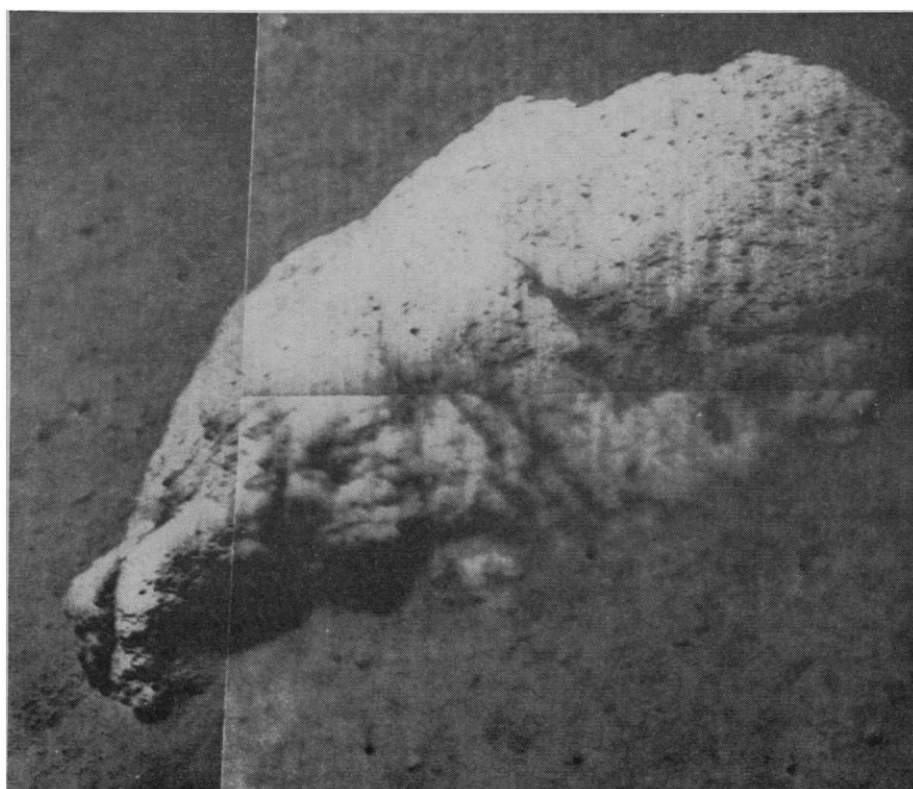


Fig. 20. Rock approximately 0.5 m long, southeast of spacecraft. Dark spots are pores or cavities.

Table 3. Location of two possible solutions for the landing site of Surveyor I on the basis of horizon features in the landscape.

Site	South latitude (deg)	West longitude (deg)
I	2.15	43.35
II	2.49	43.32

furthermore, at different angles of solar illumination. The fine texture and very shallow relief features are best shown by glancing solar illumination, whereas differences in albedo and color are best determined when the Sun is high, or when the phase angle of a given image element is very small. Although 4000 pictures have been acquired already, the photographic data are far from complete, and many thousands more pictures will be needed to investigate thoroughly the features of interest in the field of view.

*Location of the spacecraft from landscape features on the horizon.* At least six features in the Surveyor panorama pictures can be identified as elevated terrain lying at a greater distance than the ordinary near horizon of about 2 km; a low mountain ridge to the northeast is the outstanding example. The ordinary near horizon in front of the distant features can generally be identified as a relatively sharp demarcation between the foreground and the distant elevated terrain, which is brighter and smoother in silhouette. All the distant features recognized are concentrated in the northern part of the horizon. Figure 16 shows a mosaic of the horizon between northwest and northeast, with the features identified; their characteristics are summarized in Table 2.

The distant-horizon features are consistent with the general location of the landing site in the northeast portion of a plain north of Flamsteed, encircled by hills and low mountains. In this area are several specific sites in a circular region, approximately 7 km in radius, from which most of the observed features can be explained by telescopically observed local lunar topography; Table 3 gives the location of two of the sites. Figure 17 shows the location of these sites on a Lunar Chart and illustrates, for the case of site I, the degree to which the horizon features observed by Surveyor can be explained by known mountains. Site II coincides with the site deduced from trajectory tracking data; it is presented in Fig. 17 with an ellipse showing the  $2\text{-}\sigma$  uncer-

tainty in its location based on a preliminary reduction of the tracking data. Among the sites studied, site I appears somewhat preferable from known features of the lunar landscape; it best explains the most prominent feature A, even though the two minor features C and E are not explained in detail.

At present, it is not clear whether the disagreement (about 5 km outside the  $2\text{-}\sigma$  error ellipse of the solution obtained from tracking) between the site deduced from trajectory tracking and the preferred site determined from topography is to be taken as a cause for concern. It is to be expected that later pictures of the horizon features and comparison with telescopic or Lunar Orbiter photographs of this region will provide sufficient data for a much more precise location of the landing site of Surveyor with respect to known selenographic features.

*Slope of the Surveyor I landing site at the kilometer scale.* The position of the horizon on the Surveyor panoramic pictures (particularly in the narrow-angle frames), together with the calibrated camera-pointing angles, can be used to establish the local average in-

clination of the landing-site terrain relative to the spacecraft axis. This inclination can be determined to a fraction of a degree, and, if the horizon is relatively distant, applies on a kilometer scale.

Observations of the horizon positions can be converted to true slopes of the terrain once the attitude of the spacecraft relative to the local astronomical vertical is known. This is determined, in turn, by using the television camera to take star pictures. For this purpose, the camera was used in an open-shutter mode. The relatively high luminance of the lunar terrain, however, resulted in a high background in daytime measurements. So far the images of two stars, Sirius and Canopus, have been obtained. Rough analog reduction of the stellar-position data shows that the spacecraft axis is tilted from the astronomical vertical by  $1.7 \pm 0.5$  deg in a direction a little south of east. Repeated observations of points on the horizon show that the spacecraft cannot have shifted attitude more than a few tenths of a degree since the first day after landing. Observation of the landing pads suggests that they penetrated the surface

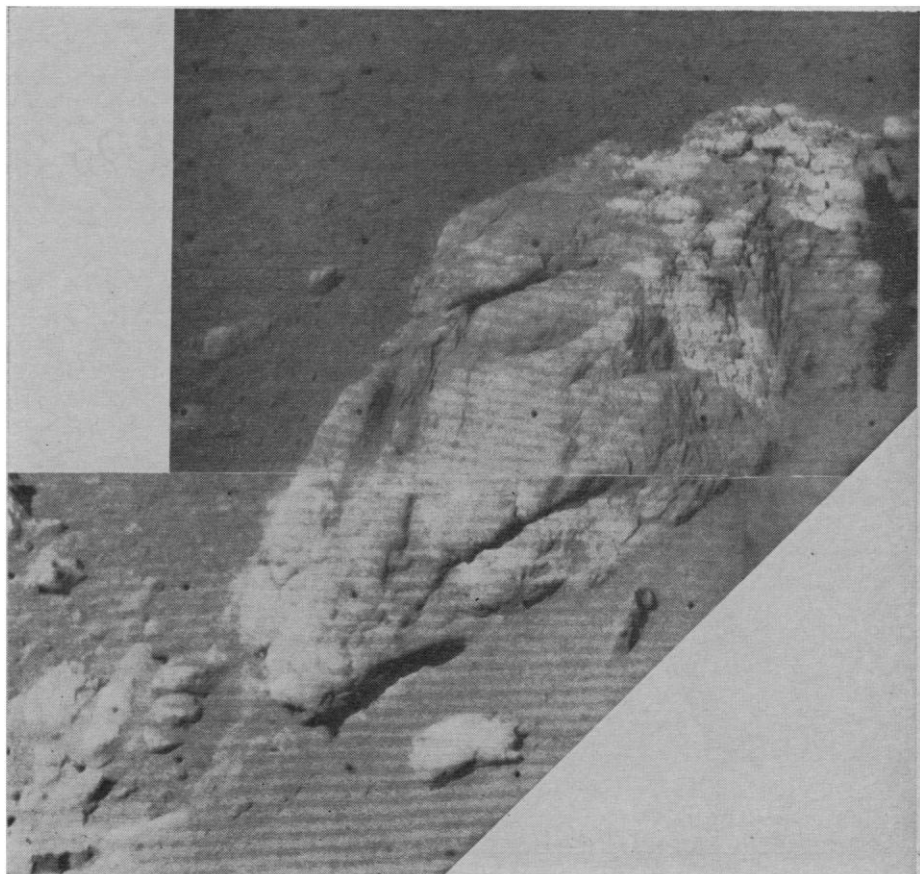


Fig. 21. Block with rounded edges and associated fragments, southwest of spacecraft. Note mottling and fractures on main block.

nearly equally; this finding implies that the spacecraft tilt is close to the slope of the lunar surface immediately beneath the craft.

Detailed examination of the horizon positions, corrected for this spacecraft tilt, has been made for 65 directions over a range in azimuth of 250 deg extending from the north to the southwest. The results show that the Moon, at the landing site, is both relatively smooth and nearly level on a kilometer scale. The standard deviation of the angle to the horizon is only 0.7 deg. The average horizon position in the three quadrants examined is the same

within 0.5 deg. More refined treatment of the observations can be expected to reduce the standard deviation.

*General morphology and structure of terrain around the craft.* Surveyor I is resting on a part of Oceanus Procellarum, partially enclosed within a circle of hills and small mountains, on the rim crest of an ancient crater that is almost completely buried beneath the mare material of the Oceanus. This ancient crater is about 100 km in diameter. The landing site is along the east border of a dark patch on the mare surface, which is the smoothest part of the mare within the mountain circle.

The nearest small crater that can be easily resolved by telescope is about 1 km in diameter and lies about 10 km to the east of our best estimate of the landing site.

The terrain within 1 to 2 km of the landing site, as observed from the Surveyor pictures, is a gently rolling surface studded with craters ranging in diameter from a few centimeters to several hundred meters. Several craters that probably range in size from a little less than 100 m to perhaps as much as 0.5 km have been recognized along the horizon; their true diameters cannot be accurately estimated; they range in angular width from about 15 to 36 deg. One of these craters, which lies slightly south of east of the spacecraft, has a prominent raised rim about 5 to 10 m high (Fig. 18). The exterior slopes of this crater rim exhibit a maximum inclination to the horizon of about 11.5 deg. The visible rim crest and exterior slopes of the rim are strewn with coarse blocky debris. Two larger but more distant craters southeast of the spacecraft have relatively low, inconspicuous rims, although patches of coarse blocks can be seen very close to the horizon on the rim of one of these craters.

About 20 craters that range in diameter from about 3 to 100 m have been recognized in the field of view below the horizon; these craters have been observed only under relatively high solar illumination, and more craters of comparable size will probably be recognized at low Sun angles. One of the most prominent of these larger craters (Fig. 19), which lies about 11 m from the spacecraft, is about 3 m wide and about 70 cm in depth; it has a distinct but irregular raised rim and a lumpy-appearing inner wall that slopes somewhat less than 28 deg. Most of the other craters in the size range of 3 to 20 m have low, rounded, inconspicuous rims or are rimless. The larger craters, taken together, resemble in distribution and form the craters of equivalent size observed in the Ranger photographs of Mare Cognitum and Mare Tranquillitatis.

The smaller craters, ranging in diam-

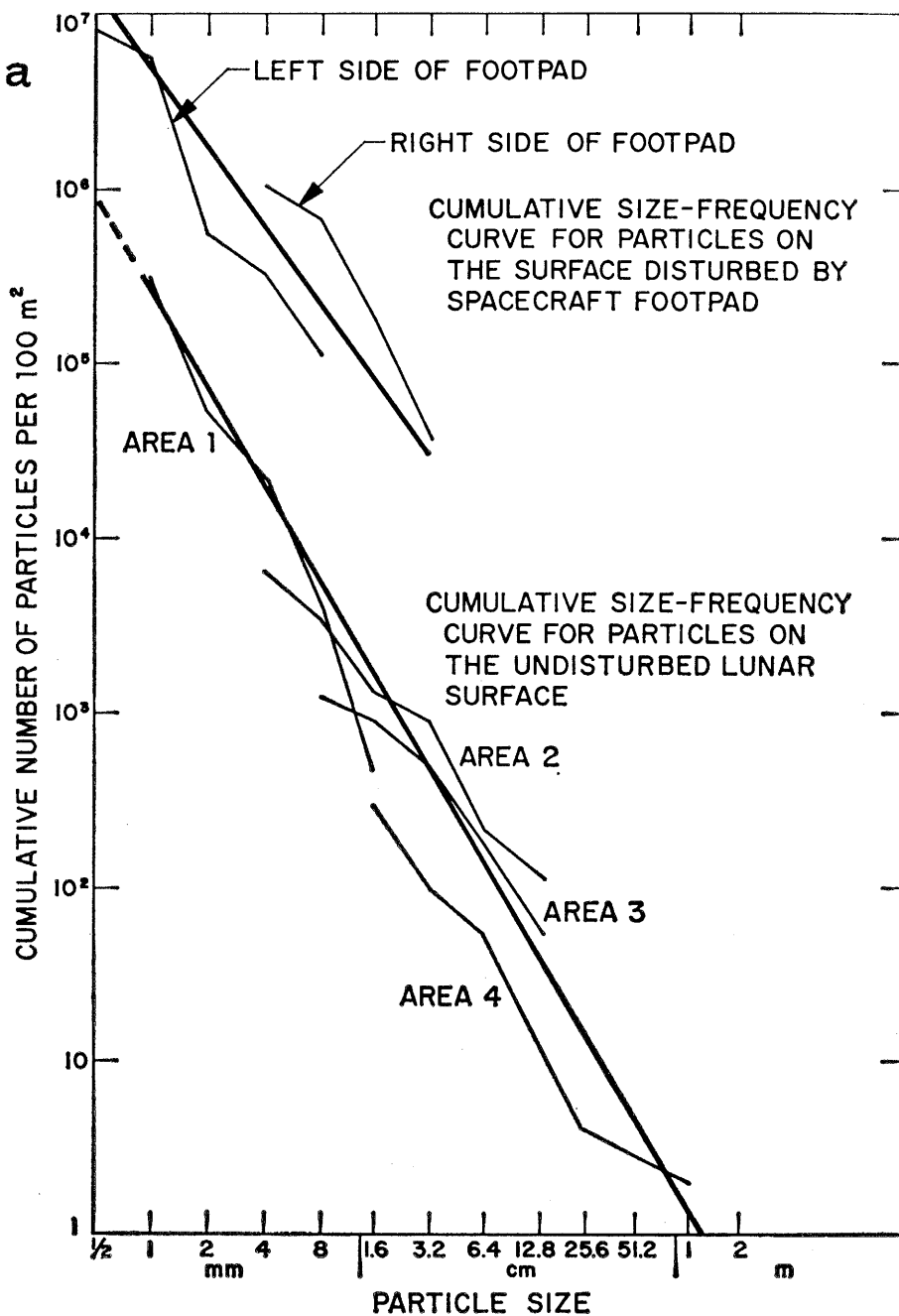


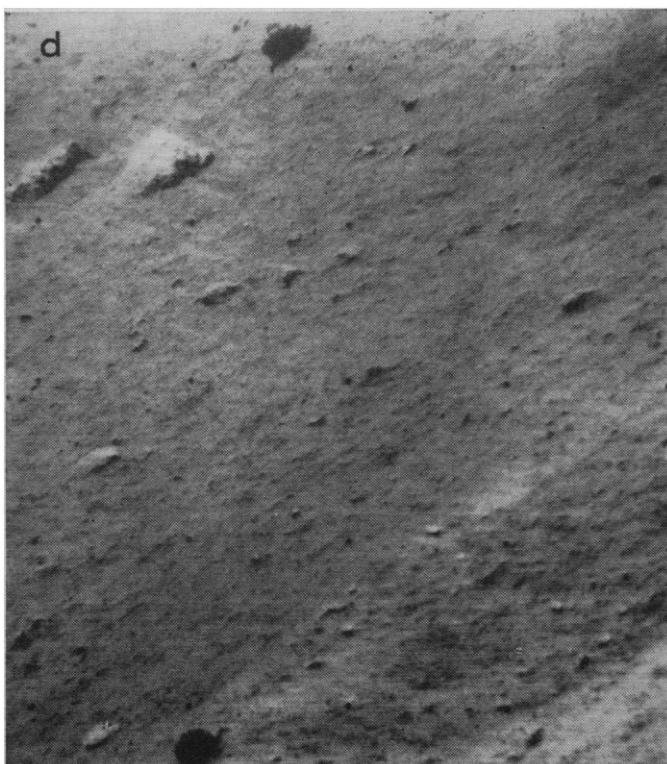
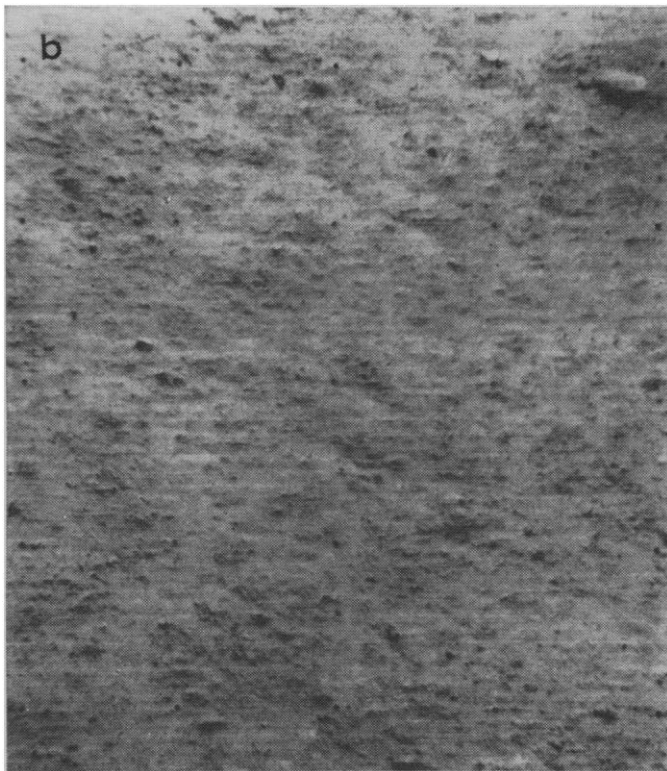
Fig. 22 (left). Cumulative frequency distribution of particles on the lunar surface determined from Surveyor I observation photographs. (Opposite page) (b), area 1, is 0.23 m<sup>2</sup>; (c), area 2, is 0.90 m<sup>2</sup>; (d), area 3, is 3.5 m<sup>2</sup>; (e), area 4, is 50 m<sup>2</sup> in foreground only.

eter from a few centimeters to 3 m, are generally shallow and difficult to observe under high solar illumination. Most of them either have low rounded rims or are apparently rimless. Where they can be observed, close to the spacecraft, they are relatively closely spaced and may cover as much as 50

percent of the surface. More details on their size, shape, and spatial distribution are expected to come from pictures that will be taken in the late lunar afternoon.

*Distribution of blocks and coarser debris.* The surface in the vicinity of the spacecraft is littered with coarse

blocks and fragments. Most of the more prominent blocks in the field of view appear to have a nearly random distribution over the surface, but significant concentrations of blocks and finer rubble occur in certain locations. A strewn field of very coarse, relatively closely spaced blocks surrounds the



Areas: 1, (b); 2, (c); 3, (d); and 4, (e).

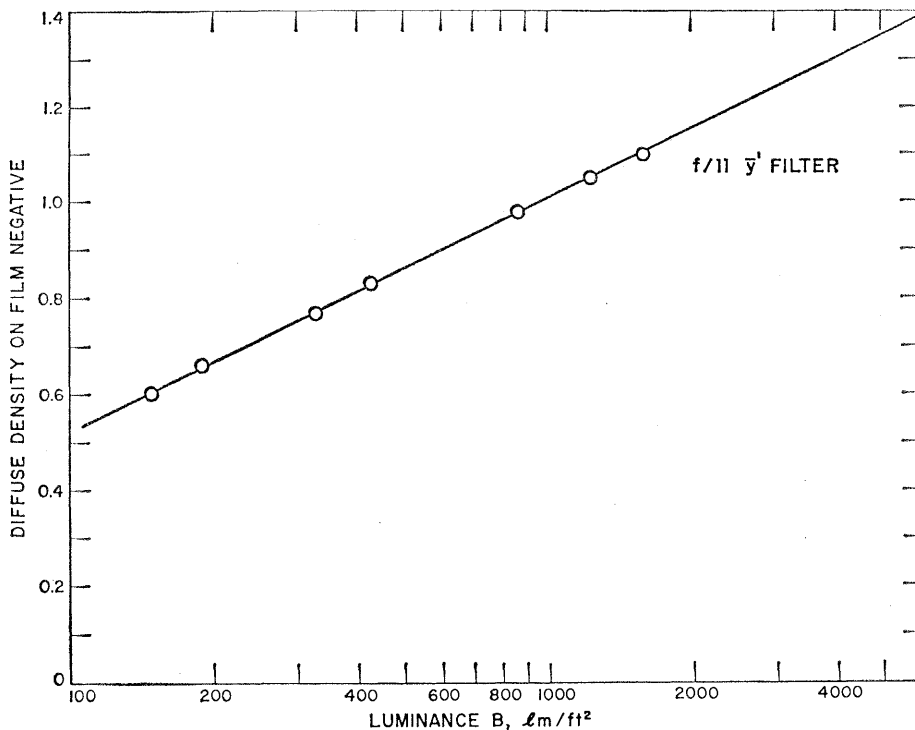


Fig. 23. Total television system transfer characteristic function determined from observation of the photometric target on the spacecraft leg during lunar operation.

crater noted on the eastern horizon (Fig. 18). This field extends from the rim crest of the crater out to a distance of about one crater diameter in each direction along the horizon. It is highly probable that the large majority of these blocks are a part of a more or less continuous blanket of ejected debris surrounding the crater, and that most of these blocks have been derived from within the crater.

A fairly large number of the blocks observed on the horizon formed by the crest of the crater rim have angular widths as great as 15 minutes of arc. If the rim of the crater is as much as 300 m or more from the spacecraft, blocks with these angular dimensions must all be more than 1 m across. Other blocks, associated with an even more distant crater rim, also are probably more than 1 m across; some of them have angular widths of more than 20 minutes of arc.

In the foreground and middle distance are scattered patches of rubble with an average grain size much less than that of the nearby coarser blocks but significantly greater than the average resolvable grain size of nearby parts of the surface. These patches resemble flattened piles of rubble derived from the slow-speed impact of weakly coherent material thrown out of experi-

mental craters produced by explosion and impact on Earth. Some of the patches around Surveyor I occur within the shallow depressions, which may be secondary-impact craters.

More of the coarser blocks scattered about the surface appear to be equant in shape and are angular to subangular; a small number are subrounded. The majority of the angular blocks appear to rest on the surface, with perhaps 80 to 90 percent of their bulk above the surface. Many of the round blocks seem to be partially buried; in some instances perhaps 50 percent or more of the block is below the surface. None of the fragments or blocks are seen to rest on pedestals, as has been suggested by some Soviet scientists on the basis of the Luna 9 photographs.

The angular blocks, especially those on the rim of the prominent crater on the eastern horizon, are typically faceted as though broken along joints and pre-existing fractures. Some of the large blocks along the horizon appear to be resting atop the surface and have demonstrable overhangs (Fig. 18); these blocks must have substantial cohesion and shear strength, especially if they have arrived in their present position by ejection from the crater. The very large majority of the coarser blocks have, in addition, a demonstrably higher

albedo than most of the rest of the lunar surface in the field of view; this is particularly noticeable under high Sun, when the blocks stand out prominently as bright spots. These data suggest that the blocks are composed of material somewhat different physically from the general, finer-grained matrix of the lunar surface, and that most of them consist of relatively strong single pieces of rock.

Two blocks relatively close to the spacecraft are of special interest: One of them (Fig. 20), about 0.5 m across, lies some 5 m southeast; the other (Fig. 21), slightly more than 0.5 m across, about 5 m southwest of the camera. The rock to the southeast is distinctly rounded on its upper side, although it is faceted in places and has overhangs on the side facing the camera. The narrow-angle frames show that the block is distinctly marked with closely spaced dark spots a few millimeters across. Most of the spots are clearly shadows within pores or cavities in the rock surface; they are so close in size to the resolution limit of the pictures that the character of the cavities cannot be determined with confidence; they may be intergranular pore spaces in a relatively coarse-grained rock, or they may be vesicles. The spots exhibit a distinct elongation and pattern, however, that resemble those produced by flowage and distortion of vesicles in a volcanic rock. It seems quite possible that the block observed is a rock congealed from a gaseous melt; such a melt could have been produced by either strong shock or volcanism, and the rock could be an impactite, a volcanic bomb, or a fragment from the top of a vesicular lava flow.

The second block close to the spacecraft is quite different from the first. It is angular in shape, with well developed facets that are slightly rounded at the corners and at the edges. This block appears to be devoid of resolvable granularity but it is distinctively mottled; the lighter parts of the block tend to stand out as small knobs. The block has the appearance of being somewhat eroded, and the brighter knobs may stand out as a result of differential erosion. One of the most striking things about this block is a very pronounced set of fractures that appear to intersect and that resemble the cleavage planes produced during plastic flow of rock under moderately high shock pressure. An-

other striking feature is that the block lies in a swarm of somewhat similar, smaller fragments that are strewn out in the direction of elongation of the main block; at least 50 separate pieces are present in the swarm. Many of these fragments and part of the base of the block appear to be partially buried in the lunar surface, but a few fragments seem to rest on the surface. The impression conveyed is that the main piece has broken up, perhaps on impact with the surface, and that it may have relatively low shear strength. No impact or skid marks are observable around the block or pieces, however. The swarm of fragments may have been lying on the surface for a long time and been partially buried by younger, finer debris.

*Size distribution of debris on the lunar surface and the characteristics of the fine matrix.* The spacecraft appears to be located in a relatively representative part of the terrain in the field of view, and a first attempt has been made to evaluate the size-frequency distribution of fragments making up the observable lunar surface from a series of narrow-angle pictures of small areas relatively near the spacecraft. The pictures used were taken under comparatively high Sun; therefore only the more prominent grains are recognizable. It is expected that our first estimates of the size-frequency distribution will be slightly biased toward underestimation of the true average grain size.

Four sample areas (Fig. 22), 0.23, 0.90, 3.5, and 50 m<sup>2</sup> in size, were selected on the undisturbed surface; they ranged in mean distance from the camera from 2.5 to about 20 m. The areas and grain sizes were estimated by transformation of the pictures to a nominal flat surface defined as being at a base of the spacecraft footpads. All sharply formed fragments and grains that are easily recognizable in the pictures were measured and counted; these amounted to a total of 825, ranging in diameter from 1 mm to more than 1 m.

The integral frequency distribution of the grains, normalized to an area of 100 m<sup>2</sup>, for each of the sample areas is shown in Fig. 22, from which it may be seen that the sample areas selected provide overlapping coverage in resolution, and that the distribution functions of the grains in each area may be roughly described as segments

of one overall distribution function. There is clearly some heterogeneity between one small area and another, as would be expected from examination of the lunar surface within the field of view, but the general size-frequency distribution of fragments on the local lunar surface is probably fairly well estimated by the lower solid line in the figure. This line is the plot of the equation

$$N = 3 \times 10^5 y^{-1.77}$$

where  $N$  is the cumulative number of grains and  $y$  is the diameter of grains in millimeters. This function is bounded at an upper size limit of about 1 to 2 m, but probably extends to particle sizes considerably smaller than 1 mm (the limit of the observational data). One may expect to find about one block 1-m across on each 100 m<sup>2</sup> of the surface. The mean grain size of the surface material, averaged by particle mass, is probably of the order of 1 mm. The form and constants of this size-distribution function closely resemble the size-frequency distribution of fragments produced by crushing and grinding of rocks in ball mills or by repetitive impact of rock surfaces.

The matrix of the unresolved material between the grains, where observed very close to the spacecraft, shows a peculiar patchiness of albedo when observed under high Sun. These patches may be caused by successive thin deposits of very fine-grained material derived from different areas.

*Material ejected by impact of the footpads.* Around footpads 2 and 3 of the spacecraft are ray-like deposits of ejected material extending in certain directions as far as several tens of centimeters from the edge of each pad (Fig. 9). These deposits form a distinct raised ridge near each of the footpads. The ejected material differs in both albedo and texture from the material exposed on the adjacent undisturbed parts of the lunar surface. The average albedo of the ejected material is nearly 30 percent lower than that at the undisturbed surface, as estimated by methods described later. The material is composed of distinctly coarser lumps or fragments of ejecta than the adjacent undisturbed surface material.

The integral size-frequency distribution of the lumps of the ejecta by the spacecraft footpad was estimated from

two sample areas of about 100 and 50 cm<sup>2</sup>, respectively, on either side of footpad 2; a total of about 250 grains and lumps were counted. From the observed size-frequency distributions (Fig. 22) one may see that the footpad ejecta are about an order of magnitude coarser than the material of the surrounding lunar surface; these data strongly suggest that the observed lumps in the freshly ejected material are probably aggregates of much finer grains. The size distribution of the finer grains composing the aggregates is probably given by the mean size-distribution function for the general surrounding surface. In all likelihood, the lumps are only weakly consolidated and could be disaggregated into their constituent grains under modest pressure or agitation. Similar lumps that may be formed around natural impact craters are probably quickly fragmented by the ballistic rain of small particles on the lunar surface.

*Photometry and colorimetry.* One important function of the television camera is its use as a photometer. For the first time, the observable photometric function of part of the lunar surface can now be compared with the megascopic texture of the surface. Furthermore, a much more complete measure of the function can be obtained at one lunar location than from Earth-based observation, and it will be possible to test in detail the assumed symmetry or degeneracy of the photometric function.

The location of the landing site near the lunar equator enabled almost daily measurements of the surface luminance in the plane of the Sun-slope normal. The measurements were calibrated by photographing the photometric target before and after each survey. The stability of the camera between these measurements was about 10 percent. Three frames of the photometric target were selected for repeatability checks; the variation between these sequential frames was approximately 2 percent.

The photometric target was calibrated before flight by a goniophotometer, and its orientation on the spacecraft was made normal to the camera's center line of sight. The calibration data have been used in conjunction with the photometric angles of phase, incidence, and emergence to predict luminance values for each target step.

The video signal has been recorded on magnetic tape and by a flying spot

scanner-photorecorder. Control of the processing of the film has indicated that a high degree of stability exists between the film records. A transfer characteristic from such a negative to the photometric target is shown in Fig. 23. The latitude of the film (SO-337) is so great that the entire video transfer characteristic may be recorded on the linear portion of the film.

As a preliminary check on the use of the camera as a photometer, the scene luminance was measured for parts of the lunar surface surrounding the pad upon which the photometric target was mounted. By fitting the measured scene luminance to the photometric function derived from the telescopic measurements of Fedorets (5), an estimate of 7.7 percent for the normal albedo was derived for the parts of the surface that appeared to be undisturbed by the pad (Fig. 9); the estimated albedo for the disturbed areas was about 2 percent lower. In general, the terrain exhibits the gross luminance values expected from the telescopically determined average of the photometric function of the maria. As further data are obtained in the lunar afternoon, the local normal albedo can be determined more precisely.

The light scattered from the spacecraft is a particular problem in evaluating the luminance of the lunar surface. Areas in the immediate vicinity of the spacecraft (within 2 m) are partly illuminated by light scattered from the spacecraft, especially at low Sun angles. The contribution of light from the spacecraft fills in the shadows to such a degree that an additional photometric target mounted on the B omniantenna was clearly discernible when the chart was averted from Sun.

Several color surveys were made with the three filters, beginning the 3rd day after touchdown; their main purpose was to ascertain whether or not there are color differences in the vicinity of the spacecraft; the data so obtained permit estimates to be made of the spectral reflectances. Again, to check and maintain the calibration of the camera-filter combination, the photometric target was observed with each filter before and after the survey (Fig. 15). Preliminary examination of the prominent mottled rock lying just southwest of the spacecraft (Fig. 21) indicates that any color differences that may be present in the surface of the rock are very small.

Much more careful processing of the video data is necessary before subtle color differences can be measured.

#### Lunar Surface Electrical Properties

Five days after the touchdown of Surveyor I, the radar signal-strength data were still under detailed analysis to determine the average radar cross section in the vicinity of the landing site. The radar frequencies used by the spacecraft were 9300, 12,900, and 13,300 Mc/sec. If it proves possible to deduce the effective reflectivity, effort will be made to calculate some of the electrical characteristics of the lunar surface. No conclusions, however, are yet warranted.

#### References and Notes

1. R. W. Shorthill and J. M. Saari, "Isotherms in the equatorial region of the totally eclipsed Moon," Rept. DI-82-0530, Boeing Geo-Astrophysics Laboratory, Seattle, Wash., April 1966.
2. A. E. Wechsler and P. E. Glaser, in *The Lunar Surface Layer*, J. W. Salisbury and P. E. Glaser, Eds. (Academic Press, New York and London, 1964), pp. 389-410.
3. L. D. Jaffe, in *ibid.*, pp. 355-80.
4. H. Knudsen, Hughes Aircraft Co., suggested working from the outer-canister temperature on compartments A and B to establish lunar-surface temperatures; M. Gram, Jet Propulsion Lab., carried out the preliminary thermal analysis.
5. V. A. Fedorets, "Photographic photometry of the lunar surface," in *Reports of the Astronomical Observatory of the Charkow State University* (1952), vol. 2.

15 June 1966

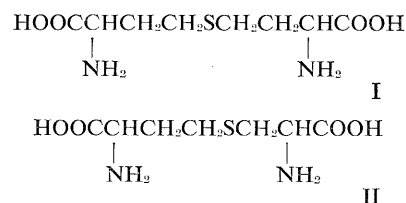
#### Homolanthionine Excretion in Homocystinuria

*Abstract. Patients with homocystinuria excrete in their urine small amounts of an amino acid indistinguishable from authentic L-homolanthionine. This compound could be formed from homocysteine and homoserine by a condensation analogous to that normally leading to cystathionine. The only other known occurrence of homolanthionine in nature is in a methionine-requiring mutant strain of Escherichia coli.*

Mudd and coworkers (1) have shown that the basic metabolic defect in patients with homocystinuria is a lack of activity of the enzyme cystathionine synthase in the liver. This enzyme, which is normally present both in liver and in brain (2), condenses homocysteine and serine to form cystathionine. Homocystinurics show, at autopsy, an absence or virtual absence of cystathionine from the brain (3),

and presumably cystathionine synthase activity is greatly reduced in their brain cells as well as in their livers.

Since in homocystinurics the major known degradative pathway of methionine metabolism is blocked at the step of cystathionine synthesis, these patients develop abnormally high blood and tissue concentrations of methionine and homocysteine, and both amino acids overflow into the urine. However, the total amounts of these sulfur amino acids and their known metabolites excreted in the urines of homocystinurics account for only a fraction of that portion of the daily dietary intake of methionine which is not utilized in protein synthesis (4). We have, therefore, searched for other ninhydrin-reactive, sulfur-containing metabolites in the urines of homocystinuric children in an effort to explain this discrepancy. We have identified one such metabolite as 5-amino-4-imidazolecarboxamide-5'-S-homocysteinylriboside (5). We now report tentative identification of another urinary metabolite as homolanthionine (I), a higher homolog of cystathionine (II).



A urine specimen containing 100 mg of creatinine was obtained from a 4-year-old mentally defective homocystinuric girl (D.S.). It was concentrated to a small volume by lyophilization, and the concentrate was applied to the surface of a column (45 by 2.16 cm) of Dowex 50 × 8, buffered with pyridine acetate at pH 3.50 (0.1M in pyridine). The same buffer was then pumped through the resin column at a flow rate of 50 ml per hour and at 50°C, and 10-ml fractions of effluent were collected. Appropriate fractions were pooled, and the volatile buffer was removed under reduced pressure on a rotary evaporator. On subsequent paper chromatography, the zone between 670 and 730 ml effluent volume contained a ninhydrin-positive compound which reacted positively to the chloroplatinate spray reagent (6). The unknown compound failed to react to sodium nitroprusside after prior exposure either to sodium cyanide or to methanolic NaOH. These reactions sug-